CHAPTER 5

SHEAR FAILURE OF FULL-SCALE SFRC BEAMS

5.1. INTRODUCTION

The tensile and shear behavior of SFRC has been studied at a material level in the previous chapters, where the benefits of incorporating steel fibers have been clearly demonstrated. The objective of this chapter is to analyze the shear failure of full-scale structural elements of SFRC. With this aim, rectangular- and T-beams of SFRC have been cast and tested. For comparison, plain concrete elements that are identical to some of the SFRC beams have also been studied.

The analysis of the experimental results involves the identification of the modes of failure, the study of the load-displacement response in the element prior to failure and the influence of the geometry of the beam section on the response.

Also, the experimental failure loads are compared with those given by existing design methods for SFRC. Finally, recommendations for design are made, including a proposal for shear design based on the equivalent shear strength from the push-off test.

5.2. REVIEW OF SHEAR DESIGN APPROACHES FOR SFRC

In terms of cross-section analysis as a fundamental step in structural design, conventional procedures are normally based on the stress-strain (σ-ε) response of the materials involved (i.e., concrete and steel) and the deformations across the critical section. Along the lines of such σ-ε approaches, the models for the behavior of SFRC have replaced those for plain concrete in the design of fiber concrete structures and the tensile response of the concrete is taken into account, instead of being neglected. A step further is the use of toughness-based limit stresses that draw on the improvement in the ductility of the concrete due to the incorporation of fibers (e.g., Moens and Nemegeer, 1991; SCA, 1995). On the other hand, the use of the fracture response or the stress versus crack opening or width (σ-w) response of SFRC has led to more general approaches for cross-section design (e.g., Stang and Olesen, 1999). Such approaches also implicitly account for size and geometry effects (Carpinteri and Massabó, 1997) that often create problems in conventional limit stress or strain based design.

In the case of the shear design of beams, the resistance offered against failure is mostly decoupled, as in conventional design, as components attributable to plain concrete, rebars and fibers. However, there is an interaction between the components, which is seen, for example, in the improvement of the dowel action of rebars due to the fibers that has been incorporated in design equations by di Prisco et al. (1994) and di Prisco and Romero (1996). Also, in many approaches the behavior of the composite SFRC has been considered instead of separating the material into concrete and fibers. Accordingly, the enhancement in the material performance of the concrete due to the incorporation of the fibers has been modeled through empirical models (Al-Taan and Al-Feel, 1990) and plasticity-based approaches (Batson and Youssef, 1994) to yield equations for the shear cracking stress and ultimate shear strength of SFRC beams.

In terms of the flexure-shear failure mechanisms, the studies of Li et al. (1992) on beams concluded that for shear spans (a/d) longer than 2.5, the failure was dominated by beam action (with failure occurring after the propagation of flexure-shear cracking) while for shorter shear spans, the arch action predominated (with crushing or splitting failure).

A model for the ultimate shear strength of beams, based on simultaneous arch and beam actions, as well as size effect, among other phenomenological aspects, was proposed by Imam et al. (1994, 1997), and verified through comparisons with extensive test results. This model was later extended to high strength SFRC (Imam and Vandewalle, 1996).

More rational approaches based directly on the tensile stress versus crack width curve have been used in design considering three failure modes: bending, shear and concentrated loading. In one methodology (Rossi, 1995; Casanova and Rossi, 1996, 1997; Casanova et al., 1997), the stress-crack width relationship is used in flexural and shear design, along with maximum allowable crack widths. Along similar lines, the structural crack widths have been predicted using the stress-crack width curve (Stang et al., 1995; Zhang and Stang, 1998). When rebars are present, their interaction with the concrete is treated as an elastic bond problem (Stang and Aarre, 1992; Stang et al., 1995). Another formulation, based on equilibrium equations, for modeling crack widths in fiber reinforced concrete with main reinforcement can be found in Brincker et al. (1995).

5.3. TEST PROGRAM

Two series of tests were performed on the SFRC beams described in Figures 5.1 and 5.2. The first series consisted of 3 beams with rectangular cross-sections (and varying depth) and 4 T-beams with different flange dimensions. The second consisted of 3 beams with rectangular cross-sections (and varying depth) and 3 T-beams with different flange depths (and same flange width). Altogether, 13 SFRC beams have been tested (6 rectangular beams and 7 T-beams). As seen in the figures, some beams were tested twice in order to verify the repeatability of the results. In addition, a set of plain concrete beams with the same dimensions and reinforcement as the 30 and 60 cm deep rectangular beams, and the T-beam with a 100 cm wide flange were also tested. The plain concrete beams will be used as a reference so the influence of the steel fibers can be identified. The fiber content, compressive strength and the shear span-to-depth ratio of the beams have been kept constant. All the beams were over-reinforced longitudinally so as to avoid flexural cracking.

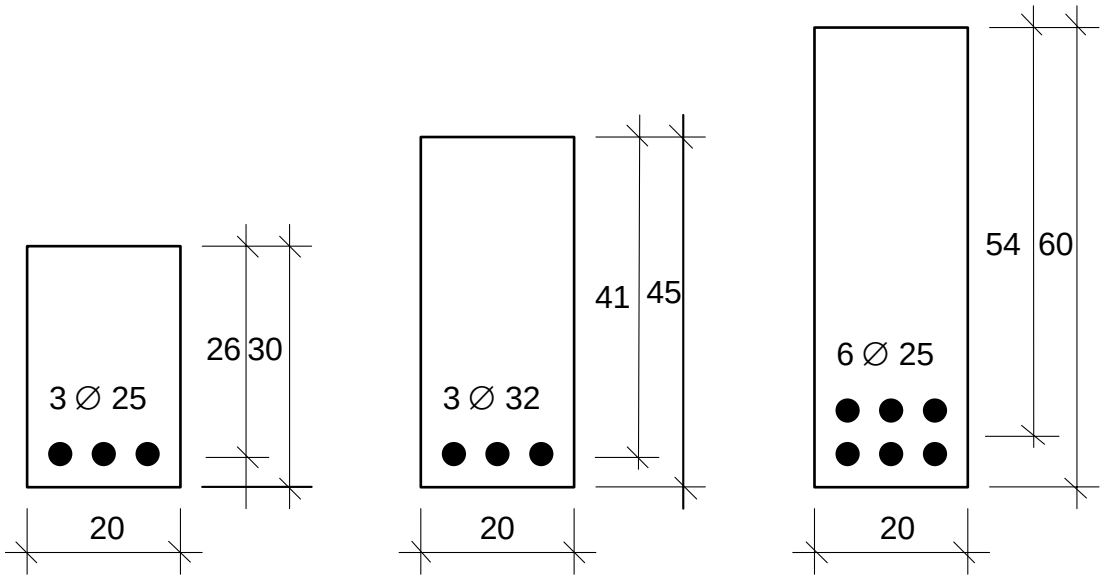

l	= 200 cm	l	= 330 cm	l	= 450 cm
a	= 91 cm	a	= 137 cm	a	= 189 cm
b	= 129 cm	b	= 193 cm	b	= 261 cm
ρ_L	= 2.83 %	ρ_L	= 3.08 %	ρ_L	= 2.73 %
k	= 1.88	k	= 1.72	k	= 1.61
k_1	= 1.34	k_1	= 1.21	k_1	= 1.06

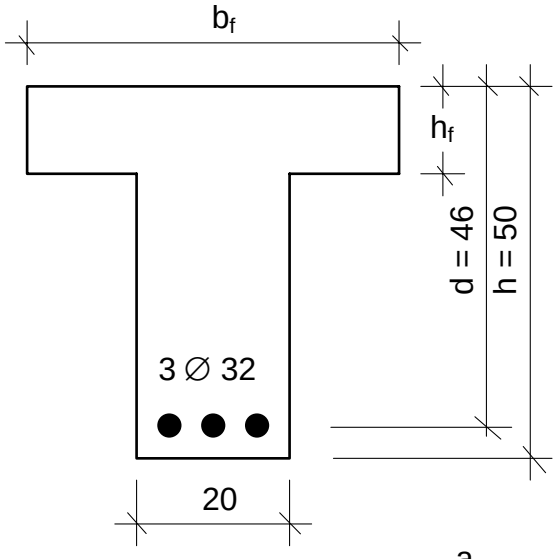

Constant

l	= 380 cm
a	= 155 cm
b	= 225 cm
ρ_L	= 2.80 %
k	= 1.66
k_1	= 1.14

Variables

h_f \ b_f	50	75	100
10	X		
15	X	X	X

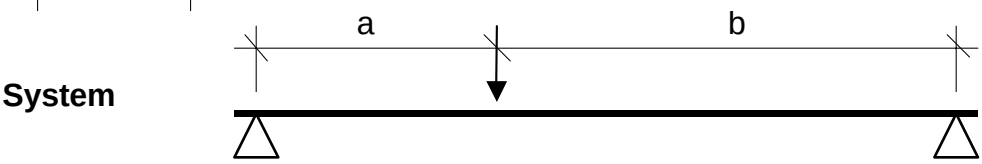

System

Constant for all beams: ρ_w = 0.00 % ρ_f = 0.50 Vol.% a/d = 3.5

Figure 5.1. Series 1. Cross-section, reinforcement and test configuration

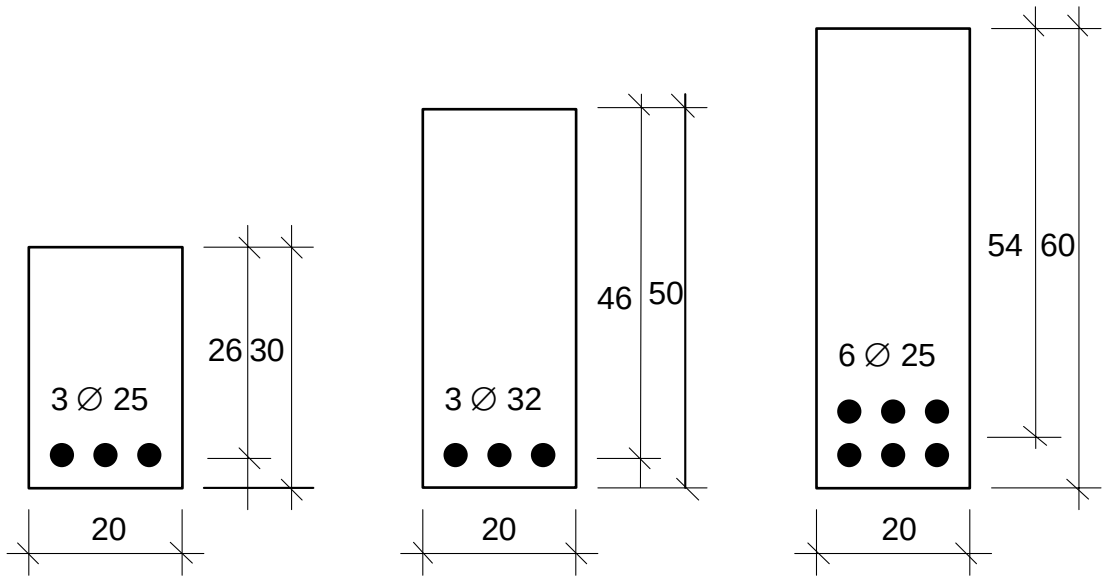

l	= 200 cm	l	= 340 cm	l	= 450 cm
a	= 91 cm	a	= 155 cm	a	= 189 cm
b	= 129 cm	b	= 185 cm	b	= 261 cm
ρ_L	= 2.83 %	ρ_L	= 2.41 %	ρ_L	= 2.73 %
k	= 1.88	k	= 1.66	k	= 1.61
k_1	= 1.34	k_1	= 1.14	k_1	= 1.06

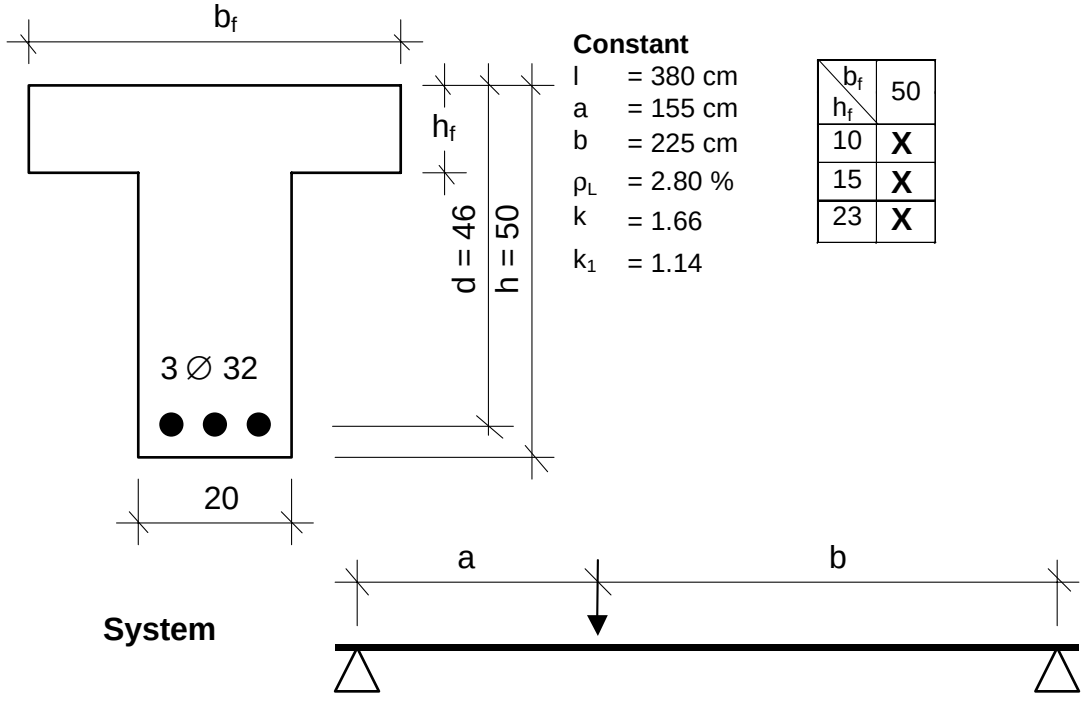

Constant

l	= 380 cm
a	= 155 cm
b	= 225 cm
ρ_L	= 2.80 %
k	= 1.66
k_1	= 1.14

h_f \ b_f	50
10	X
15	X
23	X

Constant for all beams: ρ_w = 0.00 % ρ_f = 0.50 Vol.% a/d = 3.5

Figure 5.2. Series 2. Cross-section, reinforcement and test configuration

5.3.1. Beam Characteristics

In the case of the rectangular beams (Figures 5.1 and 5.2) the variable investigated is the height (h) while the beam width (b_w) remains constant. All the beams were loaded closer to one end of the beam than the other. The shorter span (a) or the critical shear span is where the principal failure is expected to occur. The corresponding shear span-to-depth ratio (a/d) ratio is kept constant, where d is the effective depth and the length (l) of the beam is approximately equal to 8 d.

The variables studied in the case of T-beams are the height (h_f) and width (b_f) of the flange while the height (h) of the beam section remains constant. The effect of the width of the flange is mainly studied with the first set of beams (Figure 5.1) while the flange height is studied with the second (Figure 5.2).

5.3.2. Materials and Element Fabrication

A normal strength concrete with a characteristic compressive strength of 30 MPa with 40 kg/m^3 of Dramix® RC 65/60 BN s1teel fibers has been used for the study. The concrete was provided in a truck mixer from a ready-mix plant with the mix design given in Table 5.1. Table 5.2 shows the slump and 28-day compression strengths (f_c) of the plain concrete and the SFRCs. The equivalent flexural tensile strengths (f_{eq3}) of the SFRCs were determined according to the RILEM recommendation (2000,a). The two series of tests on the fiber concrete beams are denoted hereafter as SFRC-1 and SFRC-2, respectively. Note that for the first series (SFRC-1) an equivalent CMOD was considered in the calculation of $f_{eq,3}$ from the notched beam tests, taking the deflection/CMOD ratio as 0.86. For the second series (SFRC-2), $f_{eq,3}$ was directly obtained from the load-deflection response.

Table 5.1. Composition of the mix (per m^3)

Cement CEM I 42.5 R (kg)	385
Water (lit.)	168
Gravel (5-12 mm) (kg)	183
Gravel (12-25 mm) (kg)	773
Sand (0-5 mm) (kg)	851
Plasticizer (lit.)	4.6

Table 5.2. Characteristics of the concrete

Concrete	**Slump** (cm)	f_c (MPa)	$f_{eq,3}$ (MPa)
Plain concrete	23	32.1 (±2%)	-
SFRC-1	17	37.7 (±2%)	5.43 (±17%)
SFRC-2	20	38.8 (±1%)	5.58 (±12%)

The beams were filled in several layers and compacted by a combination of external vibration using a vibrating screed placed on the wooden molds, as shown in Figures 5.3 and 5.4, and needle vibration at the ends.

Figure 5.3. Filling of the molds


Figure 5.4. Compaction of the beams

Along with the full-scale beams, the following specimens for the material characterization were cast: standard 150×300 mm cylinders for the compression and uniaxial tension tests, and 150×150×600 mm prisms for the bending and push-off shear tests.

5.3.3. Experimental Details

The tests have been carried out under displacement control using a load frame anchored to a strong-floor and an MTS servo-hydraulic actuator with a loading capacity of 1 MN and an MTS TestStar controller. The test set-up can be seen in Figure 5.5. The loading rate was varied for each beam as a function of its depth to have approximately the same time to failure (of approximately 35 minutes). In order to determine the load-point deflection, displacements have been measured by means of Temposonic (magnetostrictive) transducers located below the loading point and at the supports. Also, displacements at the ends of the beams have been measured to estimate the rotations. Additionally, a rosette of three Temposonic transducers was mounted on one side of the beam, at the middle of the shear span, to study the cracking behavior (see Figure 5.5). See photographs in Figures 5.6-5.7 for more details of test set-up.

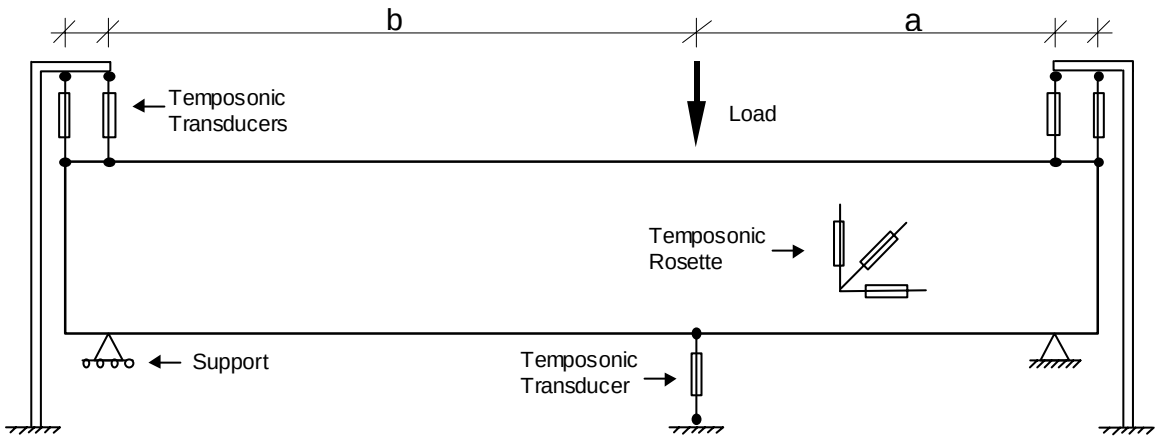

Figure 5.5. Test set up

Figure 5.6. Test configuration

Figure 5.7. Beam ready to be tested

5.4. RESULTS AND DISCUSSION

5.4.1. Modes of Failure

All rectangular and T-beams tested, in both series, failed in shear. The rectangular beams of the plain concrete failed suddenly (Figure 5.8) with the appearance of a single crack. In the plain concrete T-beam, the cracking initiated in the web within the critical shear span but, prior to failure, cracks also developed outside of the critical shear span. Some of the cracks propagated into the beam flange (Figure 5.9). In general, the failure was less brittle in the T-beams than the rectangular beams.

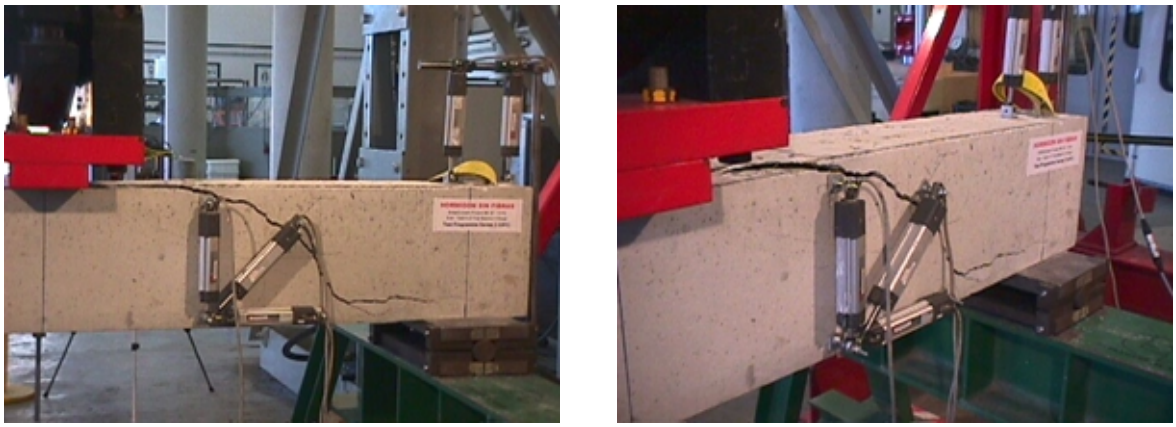

Figure 5.8. Plain concrete 20×30 rectangular beam: Final state of cracking in the critical shear span.

(a) (b)

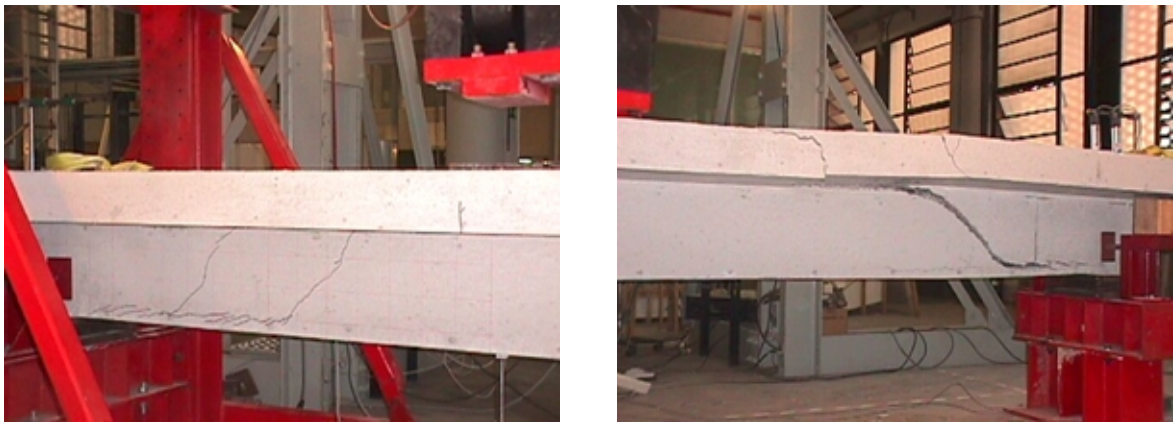

Figure 5.9. Plain concrete T-beam with 100 cm wide flange: Final state of cracking in the critical shear span (a) and on the longer span (b)

As expected, the SFRC beams exhibited a much more ductile mode of failure. Prior to the maximum load, several cracks were observed over the span of the beams.

Final failure occurs after at least some crushing in the compression zone (Figure 5.10). This occurs suddenly in the case of rectangular beams when the crack reaches the top of the beam. In the case of SFRC T-beams, the response is stable even after the maximum load, as seen in Figure 5.11.

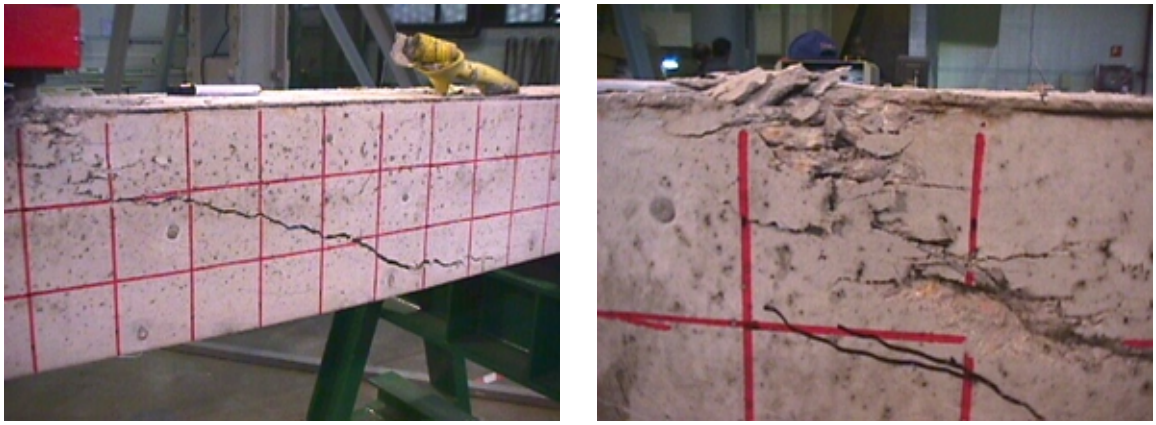

Figure 5.10. SFRC 20×30 rectangular beam: Final state of cracking in the critical shear span

(a) (b)

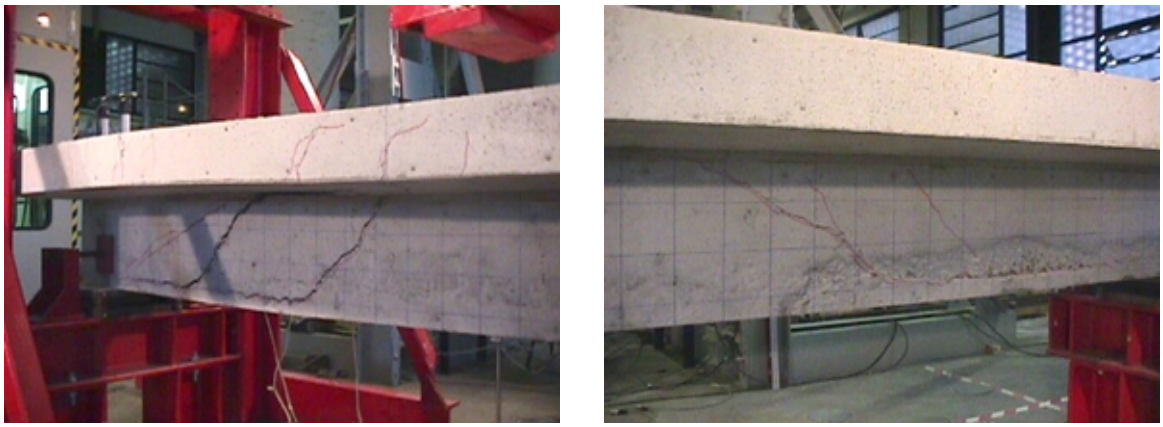

Figure 5.11. SFRC T-beam with 100 cm wide flange: Final state of cracking in the critical shear span (a) and on the longer span (b)

The typical crack patterns for the plain and SFRC beams can be seen in Figures 5.12 and 5.13 for the rectangular beams, and in Figure 5.14 for the T-beams. Individual crack patterns for all the beams can be found in Annex E, along with other test results.

(a)

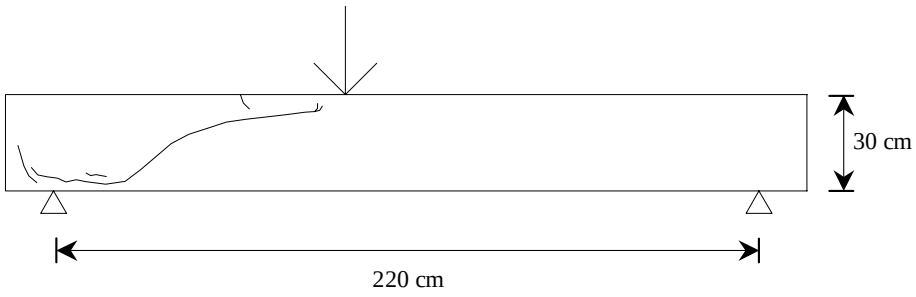

(b)

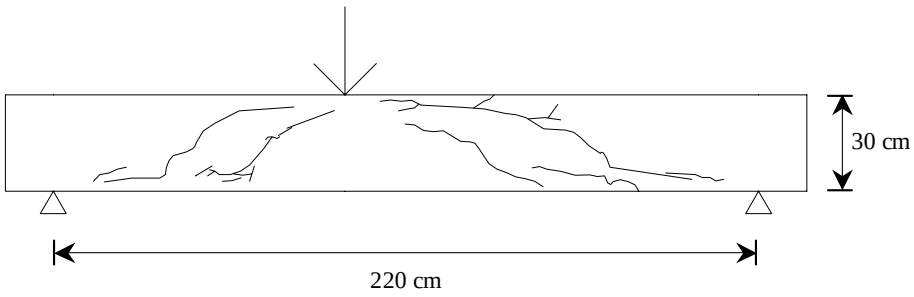

Figure 5.12. Final crack pattern in the 30 cm deep rectangular beams: (a) Plain concrete beam (b) SFRC beam of Series 1

Figure 5.12 shows the crack distribution for 20×30 cm rectangular beams. As mentioned earlier, in the case of the plain concrete beam, only one crack occurs. In the case of the SFRC beam, the first crack occurs in the critical shear span and a second crack occurs later in the longer span, leading to a multiple crack pattern. This clearly reflects the increase in the deformability of the structural element and the redistribution of the stresses due to the presence of the fibers. Note that near the tensile face the crack follows the reinforcing bars, leading to progressive fracture along the rebar-concrete interface.

(a)

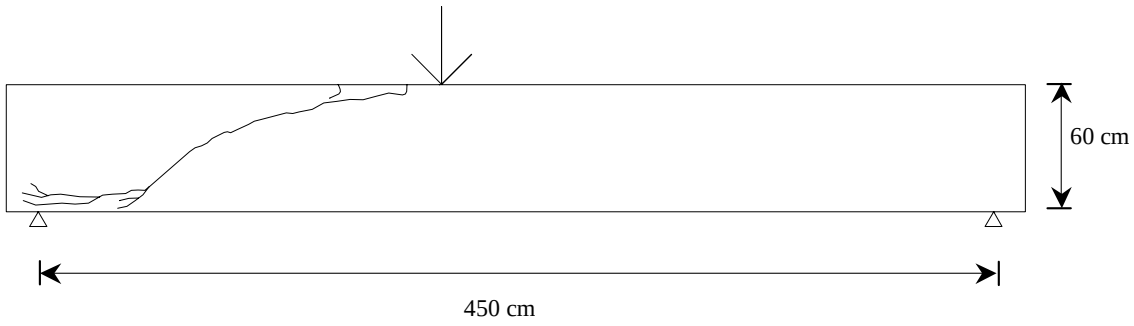

(b)

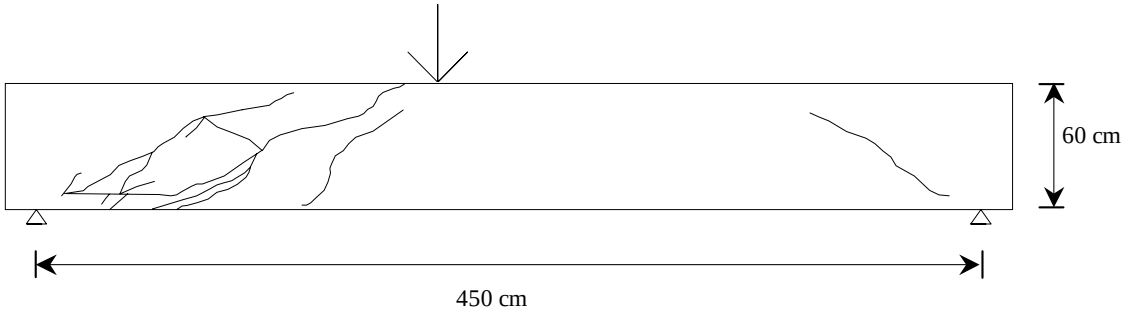

Figure 5.13. Final crack pattern in the 60 cm deep rectangular beams: (a) Plain concrete beam (b) SFRC beam of Series 2

Figure 5.13 shows the final crack pattern for 20×60 cm rectangular beams. As it can be seen, the final crack distribution in the case of the plain concrete beam is, as expected, a single diagonal shear crack formed within the shear span of the beam. Crack patterns observed in the case of the SFRC 20×60 cm rectangular beam tested in the Series 2 show a response similar to the 20×30 cm SFRC beam.

Figure 5.14 shows the crack pattern for the T-beam with a 100×15 cm flange and a 20 cm wide web. As mentioned earlier, multiple cracking occurred in both the plain concrete and SFRC T-beams. It is clear that the presence of the flange noticeably alters the crack pattern in the beam.

(a)

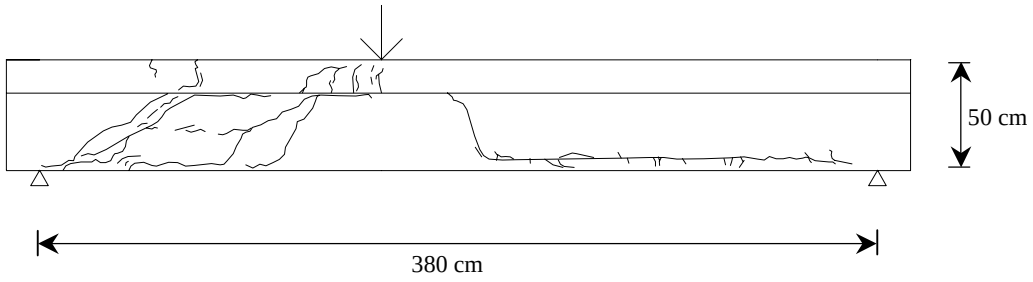

(b)

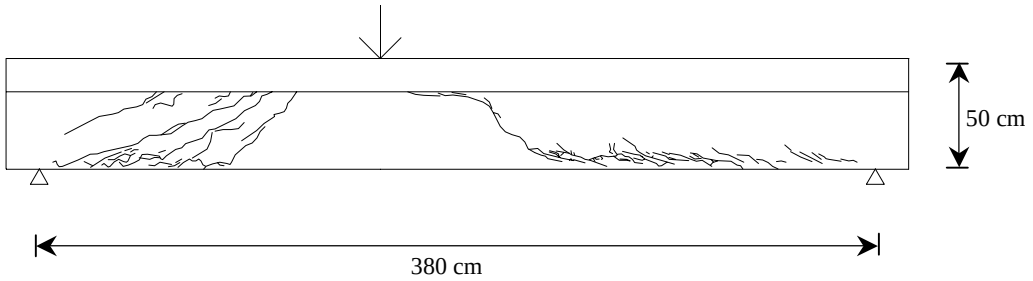

Figure 5.14. Final crack pattern for the T-beam with 15 cm deep and 100 cm wide flange: (a) Plain concrete beam (b) SFRC beam of Series 1

5.4.2. Load-Deflection Response

As mentioned earlier, the deflections below the load and at the supports were measured during each test. The net load-point deflection has been consequently determined and is used in the following discussions. The reference of each curve indicates the beam dimensions, e.g., 20×60-SFRC 1 indicates the curve of the rectangular beam of Series 1 with a 20 cm wide and 60 cm deep section. In the case of the T-beams, the legend indicates the dimensions of the flange, e.g., T15×100-SFRC 1 indicates an SFRC T-beam with a 15 cm deep and 100 cm wide flange.

Figures 5.15 and 5.16 show the results corresponding to the beams tested in Series 1, for the rectangular and T-beams, respectively. Similarly, Figures 5.17 and 5.18 show results for the rectangular and T-beams tested in Series 2. As it can be seen, all tests were

stable in the pre- and post-cracking regimes. In the case of rectangular beams (Figures 5.15 and 5.17), the response after the maximum load is not plotted since load dropped suddenly.

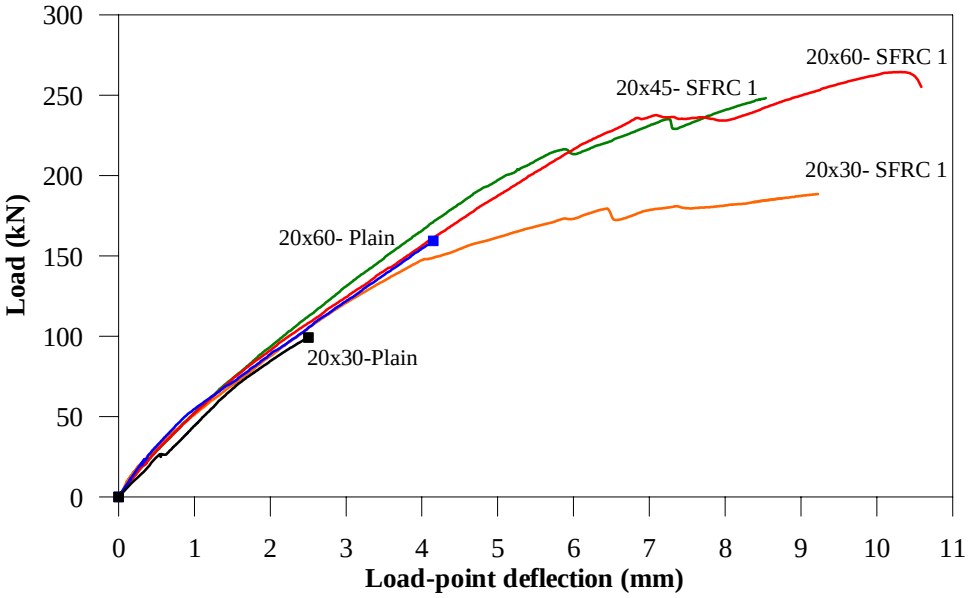

Figure 5.15. Load-deflection response: Rectangular beams of Series 1

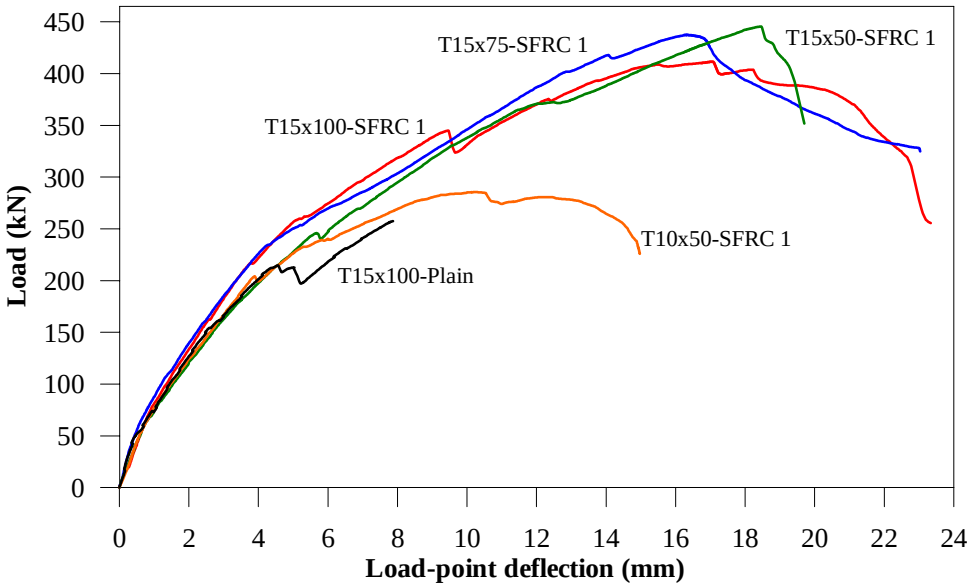

Figure 5.16. Load-deflection response: T-beams of Series 1

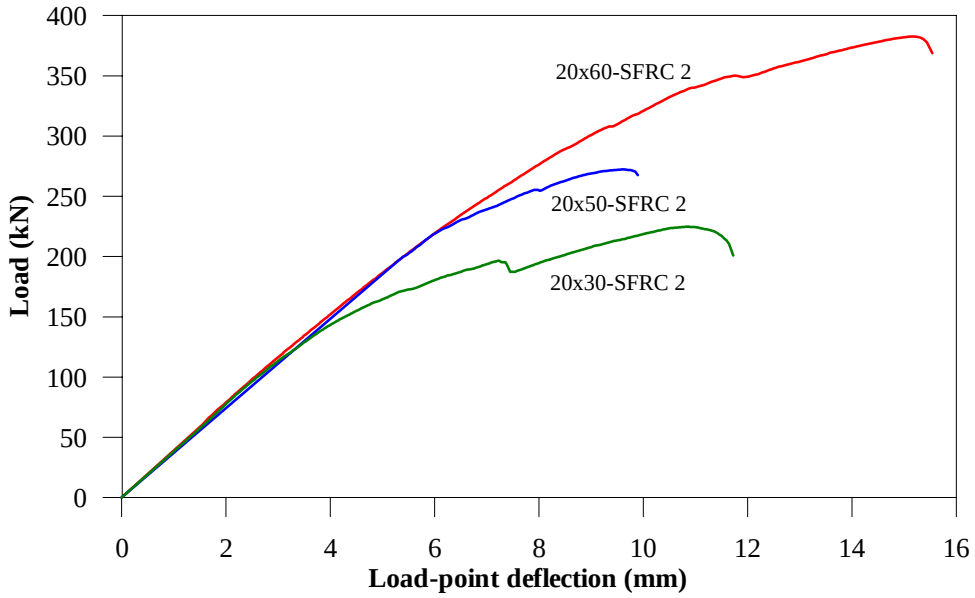

Figure 5.17. Load-deflection response: Rectangular beams of Series 2

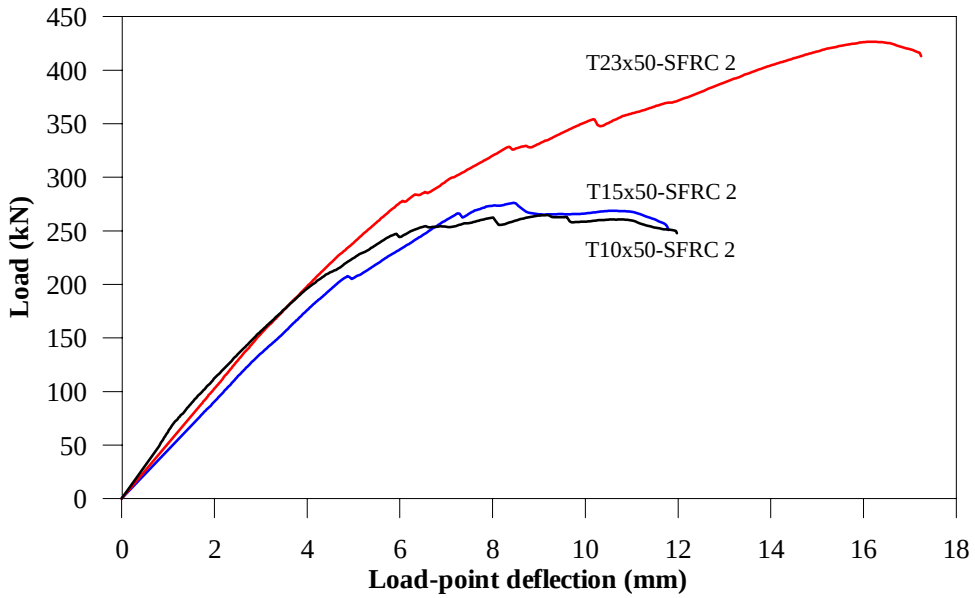

Figure 5.18. Load-deflection response: T-beams of Series 2

It is clear that when steel fibers are present, the beams resist much higher load beyond the first-crack. This effect is also seen in Table 5.3, which presents the first crack and ultimate loads, together with the corresponding deflections, for all of the specimens tested. The first crack loads were obtained by determining the first point at which there was

a significant reduction in the slope of the curve. The ultimate deflection is taken to be the load-point deflection corresponding to the peak-load. The first-crack and ultimate loads, as well as the corresponding deflections, increase significantly with the presence of the steel fibers, indicating the important enhancement in the ductility. Also, the differences between the results from identical specimens of the two series indicate that the scatter in the response is significant.

Note that the test of the 60 cm deep rectangular SFRC beam of Series 1 was stopped before complete failure occurred since the beam started to tilt laterally. This explains the lower maximum load obtained in this test when compared to the identical beam in Series 2.

Table 5.3. First-crack and ultimate loads, and deflections

Beam		**Load (kN)**		**Deflection (mm)**	
		First crack	**Ultimate Load**	**First crack**	**Ultimate Load**
20x30-Plain		102.1	102.1	2.5	2.5
20x30-SFRC	Series 1	148.8	188.7	4.1	9.3
	Series 2	196.6	224.7	7.2	10.8
20x45-SFRC	Series 1	215.8	248.5	5.8	8.6
20x50-SFRC	Series 2	255.5	272.3	7.9	9.6
20x60-Plain		186.6	186.6	5.1	5.1
20x60-SFRC	Series 1	236.0	264.5	7.6	10.3
	Series 2	307.3	382.6	9.3	15.2
T10x50-SFRC	Series 1	203.1	285.6	3.9	10.3
	Series 2	209.7	264.6	4.4	9.2
T15x50-SFRC	Series 1	241.4	445.5	5.8	18.4
	Series 2	207.8	276.1	4.9	8.5
T23x50-SFRC	Series 2	278.1	426.5	6.1	16.1
T15x75-SFRC	Series 1	255.7	437.2	5.4	16.4
T15x100-Plain		213.9	257.4	4.6	7.9
T15x100-SFRC	Series 1	263.1	411.6	5.5	17.1

5.4.3. Influence of Steel Fibers

In order to compare the plain concrete and SFRC responses, the load-deflection curves for rectangular and T-beams are plotted again in Figures 5.19 and 5.20, showing identical beams of the concrete with and without fibers.

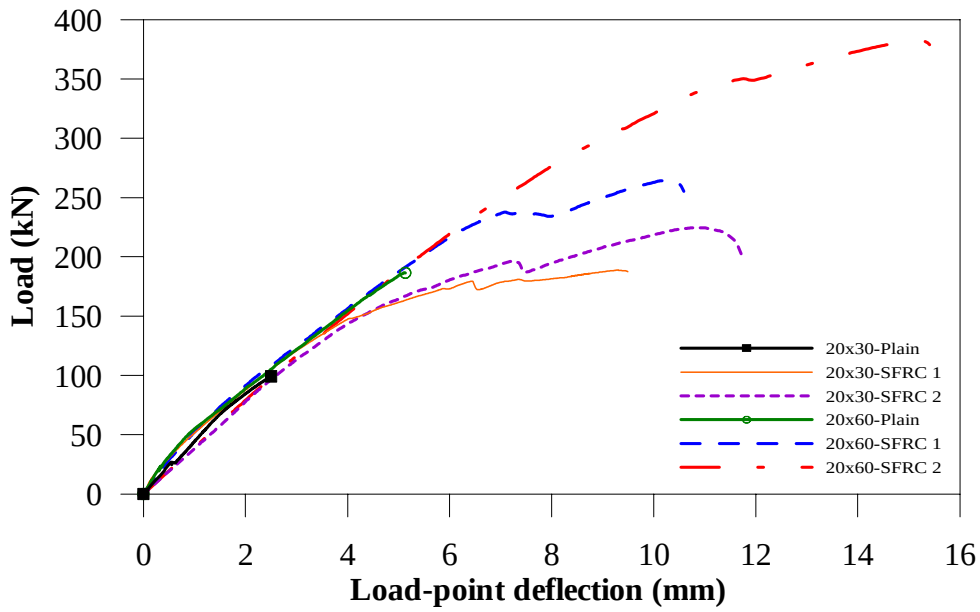

Figure 5.19. Load-deflection response: Plain and SFRC rectangular beams, Series 1 and 2

The increase in load carrying capacity and deformability due to the fibers in the rectangular beams is clear. It can be observed that the load at first-crack increases in the 30 cm and 60 cm deep rectangular beams, respectively, by 69% and 46%, on average. The ultimate load for the 30 cm and the 60 cm deep rectangular SFRC beams is also higher, on average, by about 102% and 73%, respectively, than that of the corresponding plain concrete beam. Moreover, the SFRC beams exhibit higher deflections at first-crack than the plain concrete beams; the corresponding values for the 30 and 60 cm deep rectangular SFRC beams are 127 % and 66 % higher, respectively.

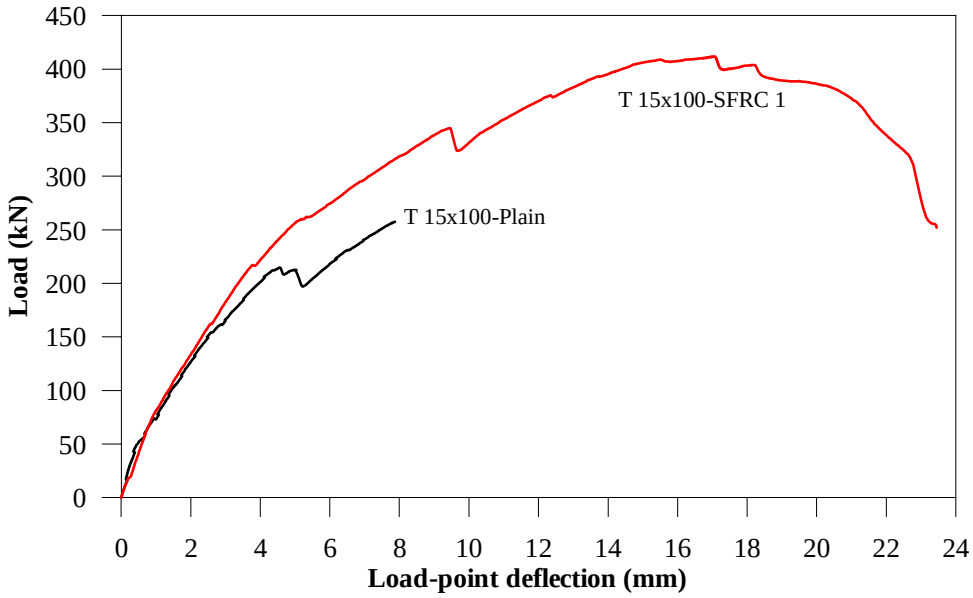

Figure 5.20. Load-deflection response: Plain and SFRC T-beams. Series 1

In the case of the T-beam with a 15×100 cm flange, the first crack load in the SFRC beam is 23% higher than that of the plain concrete beam and the maximum load is higher by 60 %. The first-crack deflection is 20 % higher in the SFRC beam than in the plain concrete beam and the deflection at maximum load is 117 % higher.

In general, the results confirm that the steel fibers lead to substantially higher ductility during the failure of a structural element in shear. Both the loads and deflections at first-crack and maximum load are higher in the SFRC beams, with higher effectiveness in the rectangular beams than in the T-beams.

5.4.4. Influence of Beam Depth

The load-deflection curves for all the rectangular SFRC beams are shown together in Figure 5.21. All the beams have approximately the same width, and length/depth, shear span/depth and longitudinal reinforcement ratios. Therefore, they can be considered as geometrically similar in two-dimensions with the beam height being the only significant variable. Note that the curve of 20×60 SFRC 1 corresponds to the test that was terminated

prematurely, as explained earlier. As expected, an increase in beam height leads to an increase in the first-crack and ultimate loads, as already seen in Table 5.3.

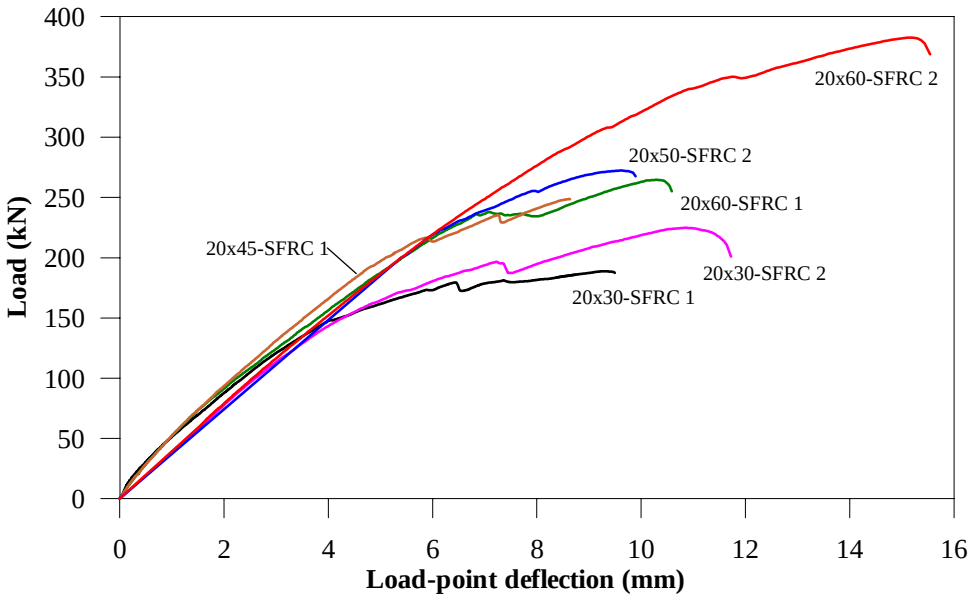

Figure 5.21. Load-deflection response: Rectangular SFRC beams

The possible effect of beam size on the nominal shear strength is examined in Figure 5.22, where the load is normalized by the cross-section area and plotted as a function of the logarithm of the beam depth. It can be seen that the normalized load decreases slightly for an increase in beam depth, denoting some size effect. The same trends are observed for the maximum and first-crack loads for SFRC and plain concrete (where the maximum and first-crack loads coincide in the latter case).

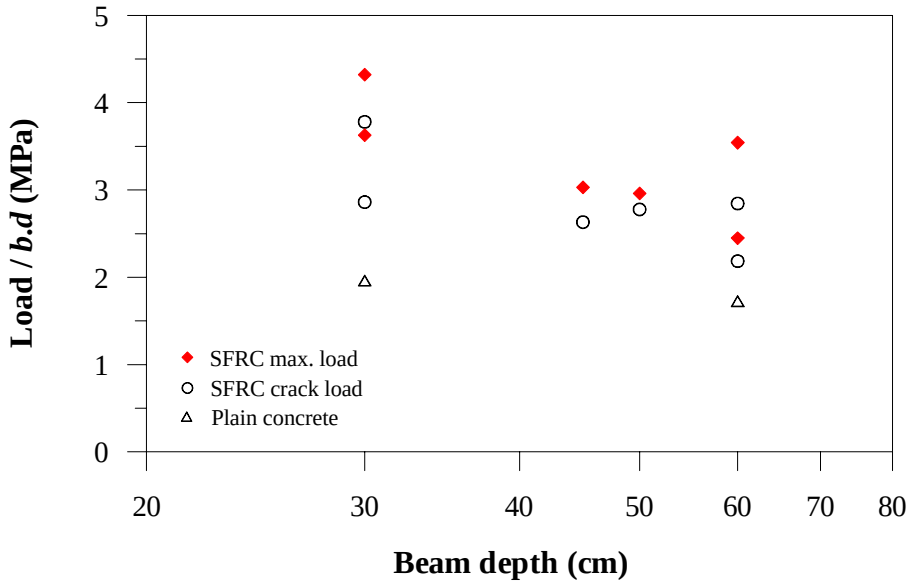

Figure 5.22. Variation of the ultimate and first crack loads with beam depth

5.4.5. Influence of Flange Width

The load-deflection responses of the SFRC T-beams with 15 cm thick flanges from Series 1 are shown in Figure 5.23. In this series, the length, height, shear-span and flange depth are the same for each beam, and the only variable is the width of the flange. As a reference, the 45 cm deep rectangular SFRC beam has also been plotted.

From Figure 5.23 and Table 5.3, the responses of the T-beams with respect to that of the 45 cm deep rectangular beam (with same length/effective depth and shear span/depth ratios) indicate that the presence of a flange increases the ultimate shear load-carrying capacity significantly.

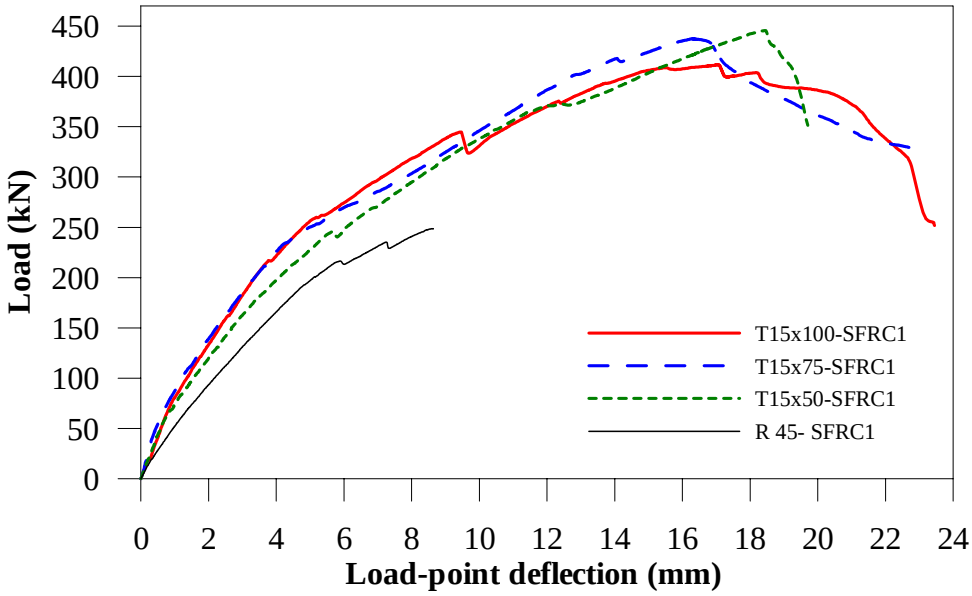

Figure 5.23. Influence of the flange width of SFRC T-beams on the load-deflection response

When the responses of the T-beams are considered with respect to each other, there is a slight increase in the first-crack load with an increase in the flange width (i.e., 241, 256 and 263 kN for 50, 75 and 100 cm flange width, respectively), as can be expected. On the other hand, the ultimate load decreases slightly with an increase in flange width (i.e., 446, 437 and 412 kN for 50, 75 and 100 cm flange width, respectively). In conclusion, it appears that the flange width does not have a significant effect on its load carrying capacity, within the range studied.

In general, the presence of the flange clearly benefits the shear resistance but the present tests do not clearly indicate the transition or the existence of a limit up to which an increase in the flange width increases the load-carrying capacity.

5.4.6. Influence of Flange Depth

Figure 5.24 shows the load-deflection responses of the SFRC T-beams tested in Series 2 with flange widths of 50 cm, and flange depths of 10, 15 and 23 cm. As a reference, the curve corresponding to the 50 cm deep rectangular beam is also shown.

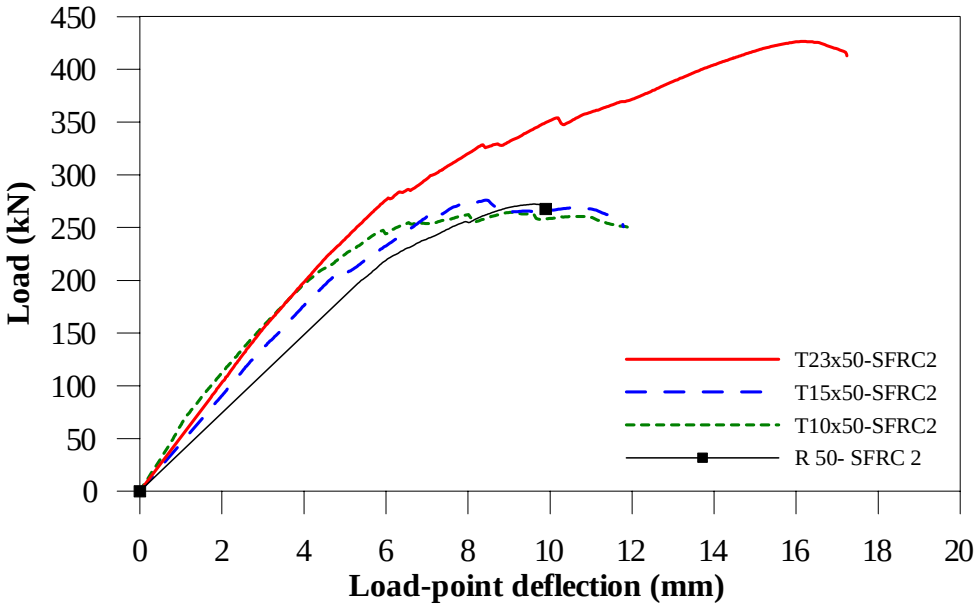

Figure 5.24. Load-deflection response: Influence of flange depth, Series 2

It can be seen from the figure and Table 5.3 that the first-crack and maximum loads and deflections are similar for the beams with flange depths of 10 and 15 cm. With respect to the response of the 50 cm deep rectangular beam, there is no significant improvement due to these flanges. On the other hand, the beam with a flange depth of 23 cm exhibits much better performance, with a first-crack load that is 34% higher and a maximum load that is 54% higher than the corresponding loads of the beam with 15 cm deep flange. Similarly, the deflections at first-crack and maximum load are higher by 24% and 90%, respectively, when compared to the beam with 15 cm deep flange.

These results suggest that there is limit in the flange depth beyond which there is a significant increase in the load-carrying capacity and ductility. However, the exact depth limit cannot be defined from limited number of tests performed here. For example, in the

tests of Series 1 (Figure 5.25 and Table 5.3) the beam with a 15 cm deep flange exhibited a 19% higher first-crack load and 56% higher maximum load than the beam with a 10 cm deep flange. Also, the first-crack deflection and the deflection at maximum load were 47% and 80% higher, respectively. However, in the tests of Series 2, there is practically no difference in the response of the beams with 10 cm and 15 cm deep flanges. Also, the difference in behavior between the 45 cm deep rectangular beam in Series 1 and the T-beams was significantly higher than that seen in Series 2 between the rectangular and the T-beams.

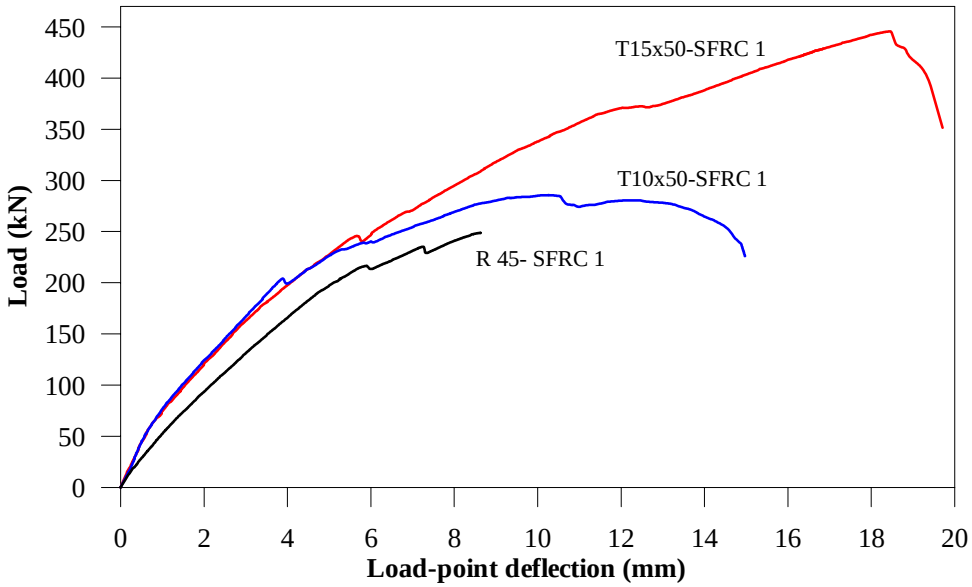

Figure 5.25. Load-deflection response: Influence of flange depth, Series 1

5.4.7. Displacements Associated with Web Cracking

As mentioned earlier, 3 Temposonic transducers were mounted at 0°, 45° and 90°, (see Figures 5.5 - 5.8) to record the displacements in the web of the beam within the critical shear span. A typical load-displacement response from the three transducers is shown in Figure 5.26, where the load-deflection response is plotted as reference. Individual responses for each beam are given in Annex E, which also presents the load-rotation

response at the load-point for each beam. The rotation is calculated using the readings obtained from the pair of Temposonic transducers placed at the ends of the beams.

From Figure 5.26, it can be seen that up to the crack load, the horizontal transducer (R 0º) gives the largest displacement, followed by the transducer placed at 45º (R 45º) and with almost no displacement for the case of the vertical transducer (R 90º), placed in the load direction. Once cracking occurs, R 45º and R 90º displacements begin to grow constantly up to the end of the test. Note that R 45º displacement is actually the crack opening of the principal crack in the critical shear span. In the case of the beam in Figure 5.26 (20×30 SFRC beam of Series 2) it can be seen that the crack did not intercept the R 0º transducer span and thus the displacement does not grow after cracking.

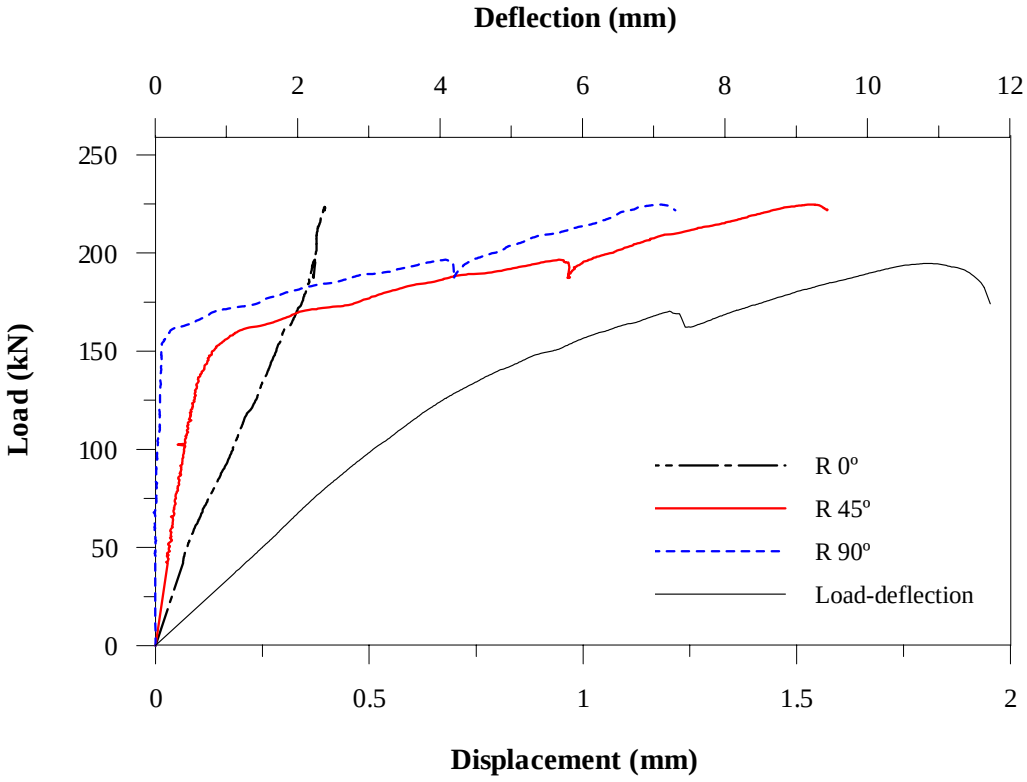

Figure 5.26. Typical load-displacement response of the rosette transducers

5.5. REVIEW OF DESIGN METHODS FOR SHEAR FAILURE OF SFRC

The existing code-type approaches for the design of SFRC beams for shear failure are based on conventional design methods supplemented by provisions for the fiber contribution. Two such methods are those given in the Dramix® design guidelines (1996) and the RILEM recommendation (2000b). On the other hand, there are design methods that are based on the fracture or development of a tensile crack, where its behavior is simulated through a stress-crack width (σ-w) relation in uniaxial tension (e.g., Casanova and Rossi, 1997). The following three sections summarize the principles of these approaches.

5.5.1 RILEM Design Method

The RILEM σ-ε design method describes the mechanical behavior of SFRC by means of a stress-strain relationship. This method gives a good opportunity to combine it easily with the design method for conventionally reinforced concrete, as recommended in Eurocode 2: ENV 1992-1-1.

The design value of the shear resistance of a general beam section is considered in this method to be a sum of the contributions of the concrete (e.g., due to aggregate interlock), the shear reinforcement (i.e., stirrups) and the steel fibers:

$$V_{Rd3} = V_{cd} + V_{fd} + V_{wd} \qquad \text{(eq. 5.1)}$$

where:

$\boldsymbol{V_{cd}}$ is the shear resistance of the member without shear reinforcement:

$$V_{cd} = \left[0.12k\left(100\rho_l f_{fck}\right)^{\frac{1}{3}} + 0.15\sigma_{cp} \right] b_w d \quad \text{(N)} \qquad \text{(eq. 5.2)}$$

with

$$k = 1 + \sqrt{\frac{200}{d}} \qquad (d \text{ in mm}) \text{ and } k \leq 2 \qquad \text{(eq. 5.3)}$$

$$\rho_l = \frac{A_s}{b_w d} \leq 2\% \qquad \text{(eq. 5.4)}$$

A_s = area of reinforcement exceeding not less than 'd + anchorage length' beyond the section considered (mm^2)

b_w = minimum width of the section over the effective depth d (mm)

$$\sigma_{cp} = \frac{N_{Sd}}{A_c} \quad (N/mm^2) \qquad \text{(eq. 5.5)}$$

N_{sd} = longitudinal force in section due to loading or prestressing (compression: positive) (N). In the case of prestressing, "h" should be used instead of "d" in the formula (eq. 2).

$\boldsymbol{V_{fd}}$ is the contribution of the steel fiber shear reinforcement, given by:

$$V_{fd} = k_f\, k_1\, \tau_{fd}\, b_w\, d \qquad (N) \qquad \text{(eq. 5.6)}$$

where:

k_f = factor for taking into account the contribution of the flanges in a T-section:

$$k_f = 1 + n \left(\frac{h_f}{b_w}\right)\left(\frac{h_f}{d}\right) \quad k_f \leq 1.5 \qquad \text{(eq. 5.7)}$$

h_f = height of flanges (mm)

b_f = width of flanges (mm)

b_w = width of web (mm)

$$n = \frac{b_f - b_w}{h_f} \quad \text{where } n \leq 3 \qquad n \leq \frac{3 b_w}{h_f} \qquad \text{(eq. 5.8)}$$

$$k_1 = \frac{1600 - d}{1000} \quad (d \text{ in mm}) \text{ and } k_1 \geq 1 \qquad \text{(eq. 5.9)}$$

τ_{fd} = design value of the shear strength due to steel fibers:

$$\tau_{fd} = 0.12 f_{eqk,3} \quad \text{(N/mm2)} \qquad \text{(eq. 5.10)}$$

where $f_{eqk,3}$ is the characteristic value of the equivalent flexural strength

$\boldsymbol{V_{wd}}$ is the contribution of the shear reinforcement due to stirrups and / or included bars:

$$V_{wd} = \frac{A_{sw}}{s} 0.9 d f_{ywd} (1 + \cot g\alpha) \sin\alpha \quad \text{(N)} \qquad \text{(eq. 5.11)}$$

where:

s = spacing between the shear reinforcement measured along the longitudinal axis (mm)

α = angle of the shear reinforcement with the longitudinal axis

f_{ywd} = design yield strength of the shear reinforcement (N/mm^2)

When checking against crushing of the compression struts, V_{Rd2} is given by:

$$V_{rd2} = \left(\frac{1}{2} v f_{fcd}\right) b_w 0.9 d (1 + \cot g\alpha) \quad \text{(N)} \qquad \text{(eq. 5.12)}$$

where:

$$v = 0.7 - \frac{f_{fck}}{200} \geq 0.5 \quad \text{with } f_{fck} \text{ (N/mm}^2\text{)} \qquad \text{(eq. 5.13)}$$

For vertical stirrups, or for vertical stirrups combined with inclined shear reinforcement, cot α is taken as zero.

5.5.2. Dramix® Design Method

The Dramix® guidelines are also based on the Eurocode 2: ENV 1992-1-1 and adapted for steel fiber reinforced concrete reinforced with Dramix® steel fibers. As this study involves using concrete reinforced with such fibers, this method is appropriate.

The Dramix® design method has the same equations as the RILEM method for the contributions of the concrete and the vertical or inclined shear reinforcement to the total shear capacity. The contribution of the steel fibers, V_{fd}, is given by:

$$V_{fd} = k_f \tau_{fd} b_w d \qquad \text{(eq. 5.14)}$$

where:

k_f = factor for taking into consideration the contribution of the flanges in T-sections. It is calculated according to equation (eq. 5.7).

b_w = width of the web

d = effective depth of the beam

τ_{fd} = the design value of the increase in shear strength due to the steel fibers.

The value of τ_{fd} can be calculated as:

$$\tau_{fd} = 0.54 f_{ctk,ax} \frac{R_t}{\gamma_c} \qquad \text{(eq. 5.15)}$$

where:

$\gamma_c = 1.5$

$f_{ctk,ax}$ = characteristic axial tensile strength of steel fiber reinforced concrete

$$f_{ctk,ax} = 0.7\, f_{ctm,ax} \quad \text{and} \quad f_{ctm,ax} = 0.3\, f_{ck}^{2/3}$$

$$R_t = \frac{1.1 W_f \lambda_f}{180C + W_f \lambda_f} \qquad \text{(eq. 5.16)}$$

where:

$C =$ 20

$\lambda_f =$ aspect ratio (ratio of fiber length, l_f, to the fiber diameter, d_f)

$W_f =$ weight of fibers (kg/m^3)

5.5.3. σ-*w* or Fracture-based Design Method

The shear capacity of SFRC beams with conventional longitudinal reinforcement has been analyzed in Casanova (1995), and Casanova and Rossi (1997) by considering the failure to occur due to shear crack propagation along a known plane.

As in Eurocode 2 (1992), the ultimate shear load carrying capacity, V_{rd3}, is taken as the sum of the contributions of the member without shear reinforcement V_{cd}, of the stirrups and inclined bars V_{wd} and of the steel fibers V_{fd} (as in equation 5.1). The contribution of the structural part, V_{cd} (compression zone, longitudinal reinforcement, aggregate interlock) and the corresponding to the classical transverse reinforcement, V_{wd}, can be calculated using Eurocode 2. Then, considering a rectangular cross section, Figure 5.27, of with a width b, effective depth d (as the distance from the top of the beam to the centroid of the reinforcing bars) and inner lever arm z, the fiber contribution, V_{fd}, is calculated from the design stress-crack opening relationship σ_{wd} (w) as follows:

$$V_{fd} = b.d.\overline{\sigma}_{pd}(w_m) \qquad \text{(eq. 5.17)}$$

Where the quantity $\overline{\sigma}_{pd}(w_m)$ is the mean residual stress at the crack width w_m and represents the mean value of the post-cracking stress between zero and w_m. This is:

$$\bar{\sigma}_{pd}(w_m) = \frac{1}{w_m}\int_0^{w_m} \sigma_{wd}(w)dw \qquad \text{(eq. 5.18)}$$

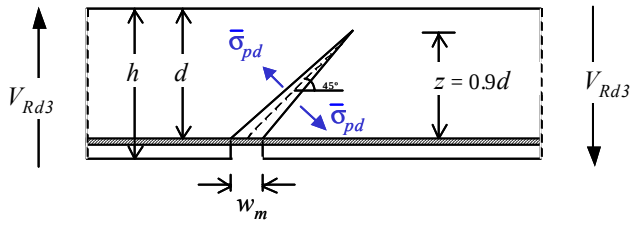

Figure 5.27. Crack geometry assumed for the σ-w method: Rectangular beam, as in Casanova and Rossi (1997)

Then, the definition of w_m is necessary since V_{fd} decreases with an increase in the maximum crack opening. Casanova and Rossi (1997), through experimental studies carried out on SFRC beams of different geometries and with conventional longitudinal reinforcing bars, have analyzed the onset of inclined cracks and the formation of concrete struts. According to their results, the spacing of these cracks is roughly equal to the inner lever arm z (z = 0.9 d) of the beam and the ultimate crack opening is proportional to the height of the beam. Since the crack opening is controlled by the longitudinal reinforcement, it is proposed that the maximum crack opening could be taken as:

$$w_m = \varepsilon_s z \qquad \text{(eq. 5.19)}$$

where ε_s is the strain of the longitudinal reinforcement.

As an example, if this strain is limited to 1%, the maximum allowable crack opening, w_m is:

$$w_m = 0.009\ d \qquad \text{(eq. 5.20)}$$

The authors also extended these design considerations to a double T-beam (Casanova, 1995). In this case, the bottom flange restrains the crack opening along the crack length (see Figure 5.28). Moreover, the crack propagates along the bottom of the

compression flange and possibly along the tension flange (if it is sufficiently deep and/or the longitudinal reinforcement ratio is high). This makes the representation of the cracking more difficult than in a rectangular beam. For calculating the contribution of the fibers in such cases, a maximum crack opening, w_m, is again considered. Then,

$$V_{fd} = b.(d\text{-}h_f).\bar{\sigma}_{pd}(w_m) \qquad \text{(eq. 5.21)}$$

where h_f is the height of the compression flange and w_m = 0.01 (d - h_f) for a strain limit of 1 % in the longitudinal rebars. Here, the crack opening limit depends on the effective depth of the beam from which the depth of the compression flange is subtracted to take into account the horizontal propagation of the crack.

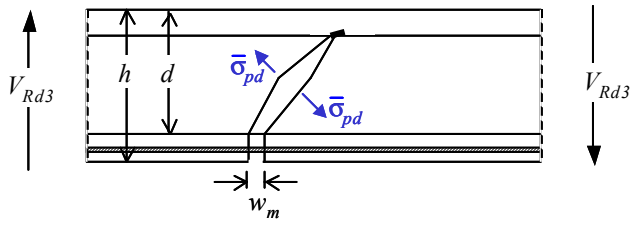

Figure 5.28. Crack geometry assumed for the σ-w method: T beam, as in Casanova and Rossi (1997)

5.6. APPLICATION OF THE DESIGN METHODS AND PROPOSED MODIFICATIONS

5.6.1. Application of the RILEM and DRAMIX Design Methods

Table 5.5 shows a comparison between the experimentally obtained values and the design values of the ultimate shear capacity (V_{Rd3}) from the RILEM and DRAMIX methods presented earlier. The concrete and steel fiber contributions (V_c and V_f) are presented separately. In the calculations, the characteristic values of the compressive strength, f_{ck}, were taken as 30 and 31 MPa for the Series 1 and 2, respectively. In the case of the RILEM design method, values of $f_{eqk,3}$= 2.67 and 3.64 MPa were used for the Series 1 and 2. For the Dramix® method, $f_{ctk,ax}$ was determined to be 2.03 and 2.07 MPa for Series

1 and 2. As a reference, the RILEM and Dramix® design methods were also applied to plain concrete beams, taking f_{ck} as 24 MPa. Due to the fact that both methods utilize the formula from Eurocode 2 to take into account the structural contribution (V_c), it can be seen that in the case of plain concrete beams both guidelines give the same ultimate shear capacity.

Table 5.4. Comparison between design and experimental shear capacities

Beam		Experimental V_u (kN)	Design loads						Experimental / Design	
			RILEM			Dramix®			RILEM	Dramix®
			V_C (kN)	V_F (kN)	V_{Rd3} (kN)	V_C (kN)	V_F (kN)	V_{Rd3} (kN)		
20×30	Plain	60	43	-	43	43	-	43	1.40	1.40
20×30	Series 1	111	46	22	68	46	20	66	1.63	1.68
20×30	Series 2	132	46	32	78	46	20	66	1.69	2.00
20×45	Series 1	146	64	31	94	64	31	94	1.55	1.55
20×50	Series 2	148	73	48	120	73	36	108	1.23	1.37
20×60	Plain	109	78	-	78	78	-	78	1.40	1.40
20×60*	Series1	154	82	36	118	82	41	122	1.31	1.26
20×60	Series 2	222	81	52	133	81	41	121	1.67	1.83
T10×50	Series 1	169	75	45	121	75	47	122	1.40	1.39
T10×50	Series 2	157	73	63	136	73	47	120	1.15	1.31
T15×50	Series 1	264	72	50	122	72	52	124	2.16	2.13
T15×50	Series 2	163	73	71	144	73	53	126	1.13	1.29
T23×50	Series 2	253	77	76	153	77	57	134	1.65	1.89
T15×75	Series 1	259	72	50	122	72	52	123	2.12	2.11
T15×100	Plain	152	67	-	67	67	-	67	2.27	2.27
T15×100	Series 1	244	78	53	131	78	58	136	1.86	1.79

* underestimated failure load due to premature termination of test

It can be seen in Table 5.4 that the RILEM method leads to satisfactory design loads. However, the safety factors (or the ratio between the experimental and design loads) are not consistent; considering that a constant experimental/calculated ratio of 1.4 - 1.5 is

expected, for the RILEM method the factors range from 1.23 to 1.69 for the rectangular beams and from 1.13 to 2.16 for the T-beams.

The Dramix® method also leads to conservative design, with the experimental/calculated ratio ranging from 1.26 to 2.00 for the rectangular beams and from 1.29 to 2.13 for the T-beams.

In general, it can be concluded that the design formulas are satisfactory for the rectangular beams. For the T-beams, the scatter makes the analysis difficult. However, it appears that for the beams with wider flanges, the limitation of k_f of 1.5 (eq. 5.6 and 5.7) leads to more conservative design.

5.6.2. Application of the Casanova-Rossi Method

For obtaining the material parameters for the concrete used in the large-scale beams, in terms of the σ-w curve, 6 uniaxial tension tests of notched cylinders were performed. Also 3 notched beam tests performed for determining the toughness parameters were inverse analyzed to get another set of σ-w curves (as in Annex D). Both tests were performed according to the procedures of Chapter 3, and the results are shown in Figure 5.29. It can be seen that the stress-crack width curves from the tension tests are much lower than obtained from the inverse analysis of the beams.

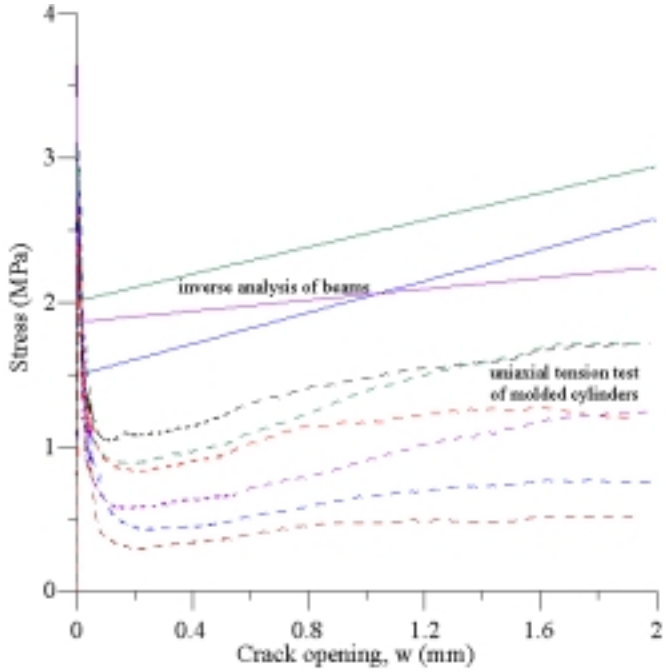

Figure 5.29. Stress-crack width curves obtained from tension tests and inverse analysis of beam test results

For applying the design method explained in section 5.4.3, a limit crack width (w_m) should be chosen. The use of the rebar strain of 1%, as in the equation 5.17 used by Casanova and Rossi, to obtain the crack width limit leads to large crack openings for the beam depths of this study. Therefore, a lower and more realistic value of 2 mm has been adopted for the predicting the shear capacity of the beams described earlier on in the chapter.

As described earlier, for the beams without stirrups and prestressing, the shear resistance is obtained from summing the contributions of the concrete element and the fibers. The contribution of the concrete is taken from the code equation but substituting the characteristic value of the compressive strength by the mean value (f_{cm}). Then eq. 5.2 changes to:

$$V_{cd} = \left[0.12k\left(100\rho_l f_{cm}\right)^{\frac{1}{3}} \right] b_w d \qquad \text{(N)} \qquad \text{(eq. 5.22)}$$

with

$$k = 1 + \sqrt{\frac{200}{d}} \qquad (d \text{ in mm}) \text{ and } k \leq 2 \qquad \text{(eq. 5.23)}$$

$$\rho_l = \frac{A_s}{b_w d} \qquad \text{(eq. 5.24)}$$

A_s = area of reinforcement exceeding not less than 'd + anchorage length' beyond the section considered (mm^2)

Using the $\bar{\sigma}_{pd}(w_m)$ values of 0.99 MPa and 2.19 MPa obtained from the uniaxial tension tests and from inverse analysis of the notched beam results respectively according to equation 5.18, the failure load (V_u) can be predicted from the other equations in section 5.4.3. Note that the value of $\bar{\sigma}_{pd}(w_m)$ at 2000 μm of crack width has been defined as $f_{eq}^{t,2000}$ in Chapter 3. The results of the analysis are given in Table 5.5, along with the experimental failure load of each beam.

Table 5.5. Comparison between predicted and experimental shear capacities

Beam		Experimental V_u (kN)	Predicted failure loads						Experimental / Predicted Vu	
			using $\bar{\sigma}_{pd}(w_m)$ from uniaxial tension tests			using $\bar{\sigma}_{pd}(w_m)$ from inverse analysis of beam test results			Uniaxial Tension	Inverse Analysis
			V_C (kN)	V_F (kN)	V_u (kN)	V_C (kN)	V_F (kN)	V_u (kN)		
20×30	Plain	60	43	-	43	43	-	43	1.40	1.40
20×30	Series 1	111	56	46	102	56	102	158	1.09	0.70
20×30	Series 2	132	56	46	102	56	102	159	1.29	0.83
20×45	Series 1	146	79	71	150	79	157	236	0.97	0.62
20×50	Series 2	148	87	82	168	87	181	268	0.88	0.55
20×60	Plain	109	78	-	78	78	-	78	1.40	1.40
20×60	Series 1	154	98	96	193	98	213	311	0.80	0.50
20×60	Series 2	222	97	94	191	97	208	305	1.16	0.73
T10×50	Series 1	169	78	75	153	78	166	244	1.10	0.69
T10×50	Series 2	157	76	71	147	76	158	233	1.07	0.67
T15×50	Series 1	264	73	61	134	73	136	209	1.97	1.26
T15×50	Series 2	163	74	62	136	74	137	211	1.20	0.77
T23×50	Series 2	253	74	49	122	74	108	182	2.07	1.39
T15×75	Series 1	259	67	61	128	67	136	203	2.02	1.28
T15×100	Plain	152	67	-	67	67	-	67	2.27	2.27
T15×100	Series 1	244	68	71	138	68	158	225	1.77	1.08

* underestimated failure load due to premature termination of test

It can be seen in Table 5.5 that the σ-*w* method generally gives reasonable predictions with the stress-crack opening curve obtained from the uniaxial tension tests while those obtained using the inverse analysis over-estimate the failure loads significantly. It appears that in this case the molded cylinders represent the concrete of the beams better than the beams. Some of the T-beam failure loads are significantly under-estimated by both approaches.

5.6.3. Modification of the σ-*w* Design Method Proposed for T-beams

As discussed by Casanova (1997) the design method given in section 5.5.3 maybe insufficient for T-beams since any possible crack propagation along the flange-web interface before failure is neglected. In the existing approach, only the tensile resistance generated by the shear crack until it reaches the flange is considered for calculating the shear resistance; a crack length of d-h_f. However, this could under-estimate the failure load when the compression flanges have a significant depth, as seen in the previous section, since the shear forces transferred across the web-flange interface are not considered. It has been observed in the tests that when the flange depth is significant compared to the effective beam depth, the crack reaches the compression flange and propagates along the web-flange interface before failure occurs (see Figure 5.30).

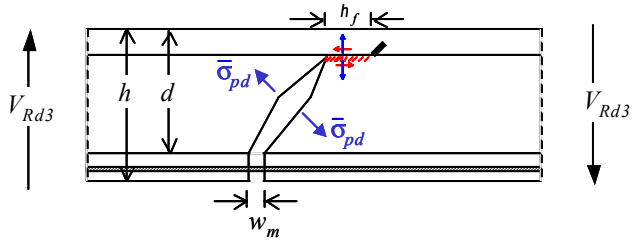

Figure 5.30. Crack geometry assumed for the modified σ-*w* method: T-beam.

In order to account for the direct shear stresses transferred due to the web-flange interface crack, it is proposed that for beams with $h_f > 0.2\ d$, an additional term (V_{dsd}) be introduced in the calculation of the shear resistance:

$$V_{Rd3} = V_{cd} + V_{fd} + V_{wd} + V_{dsd} \qquad \text{(eq. 5.25)}$$

where V_{dsd} represents the direct shear stress transfer by the web-flange crack.

For estimating this additional contribution the stress transferred by a direct shear crack is needed. For this purpose, the shear push-off test, as performed and reported in Chapter 4, is used. Assuming that similar shear and tensile forces are generated in the

fibers, the residual stress (or nominal shear stress) obtained in the direct shear push-off test at a slip of s_m, denoted as $\tau_{res,d}(s_m)$, is used to determine V_{dsd} by considering that the length of the interface crack is equal to the flange depth:

$$V_{dsd} = b_w\, h_f\, \tau_{res,d}(s_m) \qquad \text{for } h_f > 0.2\, d \qquad \text{(eq. 5.26)}$$

For the concrete corresponding to the T-beams, the value of $\tau_{res,d}(s_m)$ for a slip (s_m) of 2 mm was 1.85 MPa. Using this value in Equation 5.26, the failure loads for the T-beams with flange depths greater than 0.2 times the effective depth have been calculated and compared with the experimental results in Table 5.7.

The comparisons indicate that the estimation is better when the direct shear contribution is included, except in the case of beam T15×50- Series 2, which can be considered a statistically low result. Further tests will be needed to explore the use of such an approach in T-beam design.

Table 5.6. Experimental and calculated failure loads for T-beams with direct shear contribution

Beam	**Experimental load (kN)**	**Calculated load (kN)**
T15×50-Series 1	446	321
T15×50-Series 2	276	324
T23×50-Series 2	427	359
T15×75-Series 1	438	311
T15×100-Series 1	412	328

5.6.4. Proposed τ-*s* Design Method

As seen in the previous section, for the case of T-beams, a combination of tensile and shear stresses gives a better estimation of the shear capacity than only the tensile contribution of the fibers (Figures 5.30). Here an alternative approach using only the residual shear strength from the push-off tests at a certain slip is used to obtain the shear capacity of the beam, V_u (see Figure 5.31):

$$V_u = b.z.\bar{\tau}_{pd}(s_m) \qquad \text{with } z = 0.9\,d \qquad \text{(eq. 5.27)}$$

Where the quantity $\bar{\tau}_{pd}(s_m)$ is called the equivalent residual strength at the slip displacement s_m, and represents the mean value of stress between a slip s = 0 (at the maximum stress) and s_m. This is:

$$\bar{\tau}_{pd}(s_m) = \frac{1}{s_m}\int_0^{s_m} \tau_{sd}(s)ds \qquad \text{(eq. 5.28)}$$

where τ_{sd} is the residual stress at a slip s.

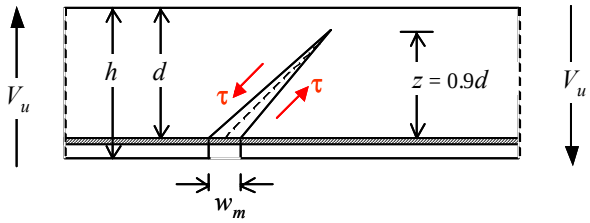

Figure 5.31. Crack geometry for the proposed τ-*s* method: Rectangular beam

Table 5.7 shows the calculated results for rectangular beams considering V_u as in equation 5.31 and a slip limit s_m= 2 mm. Experimental and calculated values are also contrasted in Figure 5.32. As it can be seen from Table 5.7, the τ-*s* method gives very good agreement with the experimental values.

Table 5.7. Experimental and Calculated values, τ-*s* Method: Rectangular beams

Beam	Experimental V_u (kN)	Calculated V_u (kN)	Experimental / Calculated
20×30-S1	111	102	1.08
20×30-S2	132	102	1.29
20×45-S1	146	157	0.93
20×50-S2	148	181	0.82
20×60-S1*	154	213	0.72
20×60-S2	222	208	1.07

* underestimated failure load due to premature termination of the test.

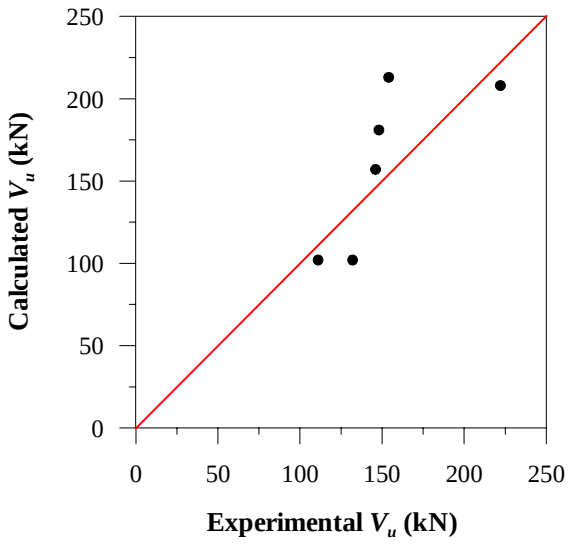

Figure 5.32. Experimental versus calculated V_u: τ-*s* design method, rectangular beams

5.7. OTHER METHODS FOR CALCULATING THE SHEAR CAPACITY

In this section, the methods proposed by Al-Ta'an and Al-Feel (1990), Campione and Mindess (1999), and Dupont and Vandewalle (2000) are applied to the present data.

Al-Ta'an and Al-Feel, calculated the total shear strength as the sum of the ultimate shear strength of a rectangular beam without web reinforcement based on the concrete compressive strength, the percentage of longitudinal tensile reinforcement, the effective beam depth, the shear span and the bond stress. The fiber contribution is calculated considering the number of fibers at the cross section in tension (i.e., the depth of the neutral axis is first calculated) and the average bond strength. The fiber pull-out length is taken to be $l_f/4$ (where l_f = fiber length) and it is supposed that all fibers will pull-out instead of breaking. Accordingly, the total shear strength of a fiber concrete beam can be calculated as:

$$v_u = v_{uc} + v_{uf}$$

where v_{uc} is the ultimate shear strength of a rectangular beam without web reinforcement and v_{uf} is the unit stress provided by the steel fibers, with:

$$v_{uc} = \sqrt[3]{10 \cdot \rho \cdot f_c \cdot d/a_s} \qquad \text{for } \frac{a_s}{d} > 2.5$$

$$v_{uc} = \sqrt[3]{160 \cdot \rho \cdot f_c} \cdot \sqrt[3]{(d/a_s)^4} \qquad \text{for } \frac{a_s}{d} < 2.5$$

where ρ = reinforcement ratio
f_c = cylinder compressive strength
d = effective depth
a_s = shear span

and

$$v_{uf} = \frac{\sigma_{cu}(h-c)}{d}$$

where c is the depth of the neutral axis and σ_{cu} is the ultimate stress sustained by a unit area of the crack at failure given by $(N \cdot f)$, where N is the number of fibers crossing a unit area of the crack and f is the average pull-out force per fiber.

Campione and Mindess proposed two empirical equations for calculating the cracking and ultimate shear strengths. The ultimate shear strength, V_{nf} (MPa), of a fiber reinforced concrete section with web reinforcement is expressed as:

$$V_{nf} = \mathrm{e} \cdot \left(0.24 \cdot f'_{spfc} + 80 \cdot \rho \cdot \frac{d}{a} \right) + 0.41 \cdot \tau \cdot \left(\frac{l_f}{\varphi} \cdot V_f \cdot d_f \right) + \frac{A_y \cdot f_{yk} \cdot d}{s} \cdot \frac{1}{b \cdot H}$$

where f'_{spfc} = split cylinder tensile strength; ρ = percentage of longitudinal tensile reinforcement; d = effective depth; a = shear span; l_f and ϕ = length and diameter of the fibers; V_f = volume percentage of fibers; d_f = an empirical factor taking into account the bond characteristics of fibers (0.5 for round fibers, 0.75 for crimped fibers and 1.00 for indented fibers); τ is the average fiber/matrix interfacial bond stress; f_{yk} = yield stress of stirrup steel; A_y = area of web reinforcement; s = spacing of the stirrups; b and H = transverse dimensions of the beams and e = 2.8 d/a.

Dupont and Vandewalle proposed a shear design formula based on the model of Bazant and Sun (1987). This approach does not separate the contribution of the concrete, the stirrups and the fibers. The shear capacity is given by the following formulae for the case of NSC.

$$V_u = 0.6 \cdot \Psi \cdot \sqrt[3]{\omega} \cdot \left[\sqrt{f_c} + 275 \cdot \sqrt{\frac{\omega}{\left(a/d \right)^5}} \right] + V_w$$

where Ψ is a size effect factor, $\Psi = \dfrac{1 + \sqrt{(5.08/d_a)}}{\sqrt{1 + d/(25 \cdot d_a)}}$

with d = effective depth
d_a = maximum aggregate size (mm)

ω = combined effect of longitudinal reinforcement and steel fibers, ω = ρ (1+4F)

with ρ = longitudinal reinforcement ratio

$$F = \left(\frac{L_F}{D_f}\right) \cdot V_F \cdot d_f$$

$\frac{L_F}{D_f}$ = aspect ratio of the fiber

V_F = volume fraction

d_f = efficiency coefficient (= 1 for hooked-ended fibers)

f_c = cylinder compressive strength

a = shear span

V_w = contribution of the stirrups; it is calculated in the same way as in the RILEM recommendation (see eq. 5.11)

The calculated values with the above methods are presented in Table 5.8 together with the experimental values. As it can be seen, the method of Campione and Mindess gives best predictions of the shear capacity. With the other two methods, the test results are underestimated significantly for the cases analyzed.

Table 5.8. Shear capacity obtained with methods of Al-Ta'an and Al-Feel, Campione and Mindess, and Dupont and Vandewalle

Beam	V_u **Experimental** (kN)	**Al-Ta'an and Al-Feel**		**Campione and Mindess**		**Dupont and Vandewalle**	
		$V_{u\,calc}$ (kN)	$V_{u\,\exp} / V_{u\,calc}$	$V_{u\,calc}$ (kN)	$V_{u\,\exp} / V_{u\,calc.}$	$V_{u\,calc}$ (kN)	$V_{u\,\exp} / V_{u\,calc}$
20×30 Series 1	111	121	0.92	97	1.14	142	0.78
20×30 Series 2	132	122	1.08	97	1.36	143	0.92
20×45 Series 1	146	186	0.79	158	0.92	215	0.68
20×50 Series 2	148	206	0.72	170	0.87	215	0.69
20×60 Series 1	154	245	0.63	200	0.77	247	0.62
20×60 Series 2	222	242	0.92	196	1.13	245	0.91

5.8. CONCLUSIONS

Tests of full-scale rectangular and T-beams have shown that the inclusion of steel fibers improves significantly the deformation characteristics, shear-load carrying capacity and first crack load of the both types of beams**.** Also, that a much greater degree of cracking occurred in SFRC beams than in plain beams, implicating more energy consumed during failure.

The failure modes and load-deflection response have been studied for plain and SFRC beams and the influence of the shape of the cross section on these issues analyzed**.** The variables considered were: the height of rectangular beams, and the width and height of the flange in the case of T-beams**.** The following points summarize the obtained results:

- Increasing the height of a rectangular SFRC beam results in an increase in the ultimate shear load-carrying capacities and first-crack loads**.** The first-crack deflections also increase with increasing height, however the ultimate-load deflections are relatively unaffected to this variation.

- For the range of flange widths studied in this project, increasing the flange width does not seem to affect the ultimate shear load-carrying capacities neither the first-crack load of the beams**.** However, the flange can result in a substantial increase of the shear capacity when comparisons are made with that of a rectangular beam**.** On the other hand, increasing the flange widths of the T-beams does not have any significant effect on the deflections of the beams produced at ultimate or first-crack load.

- Increasing the flange depth of the T-beams over a limit value results in increased ultimate shear load-carrying capacities and first-crack loads**.** The same tendency is observed for the respective deflections.

The experimentally obtained results have also been compared with those predicted by design recommendations for shear design of SFRC**.** From the comparisons carried out, the following conclusions can be drawn:

- The RILEM and Dramix® recommendations for the design of SFRC against shear failure give satisfactory results for rectangular beams**.** However, in the case of SFRC T-beams, they over-estimate the shear capacity in some cases.

- The σ-*w* design method proposed by Casanova and Rossi appears to be satisfactory for rectangular beams**.** Predictions for T-beams can be over-conservative but better results were obtained by adding a shear contribution from the fibers at the web-flange interface**.** The maximum crack width was limited to 2 mm in all cases.

Furthermore, a τ-*s* design method based on a shear toughness parameter given by the push-off shear test is proposed**.** It appears that it can predict well the direct shear capacity of rectangular beams**.** More study would be necessary to investigate its possibilities.

The shear design method proposed by Campione and Mindess has also been applied along with other methods, and its results appear to be satisfactory.